ELSEVIER

Biochimica et Biophysica Acta 1566 (2002) 44–54

BIOCHIMICA ET BIOPHYSICA ACTA
BBA

www.bba-direct.com

Review

The route of passive chloride movement across amphibian skin: localization and regulatory mechanisms

Wolfram Nagel[a,*], Petra Somieski[a], Uri Katz[b]

[a] *Physiologisches Institut, Universität München, Schillerstr. 44, München 2 D-80336, Germany*
[b] *Department of Biology, Technion Israel Institute of Technology, Haifa, Israel*

Received 30 May 2002; received in revised form 6 August 2002; accepted 14 August 2002

Abstract

Transepithelial Cl^- conductance (G^{Cl}) in amphibian skin can be activated in several species by serosa positive potentials. Mitochondria-rich cells (MRC) or tight junctions (TJ) between the epithelial cells are possible sites for this pathway. The properties and the techniques used to investigate this pathway are reviewed in the present paper. In situ techniques are preferable, since specific properties of the MRC are apparently not maintained in isolated cells. Volume measurements and electronprobe microanalysis of intracellular ions suggest the localization of voltage-activated G^{Cl} to MRC. G^{Cl} correlates poorly with the density of MRC. The vibrating voltage probe allows quantitative correlation of the local Cl^- current through morphologically identified structures and the transepithelial Cl^- current. Our analysis shows that 80% of the voltage-activated Cl^- current is accounted for by current through MRC or their immediate vicinity. The activation patterns of this current and the inhibition by the α_1-adrenergic agonist, epinephrine, conform to those of the transepithelial current. However, less than 20% of the MRC are active at a certain moment and the activity is spontaneously variable with time. The molecular nature of this pathway, physiological control mechanisms and their relation to the temporal activity of MRC remain to be studied.

Keywords: Mitochondria-rich cell; Chloride conductance; cAMP; Epinephrine; Amphibian skin; Vibrating voltage probe

The advantages of analyzing transepithelial ion transport with the short-circuiting technique introduced by Hans H. Ussing are generally known and have greatly stimulated the development of epithelial physiology. Curiously, however, precisely the classical subject of studies, the amphibian skin is faced with quite unusual conditions in Ussing chambers, where both sides of the epithelium are bathed with Ringer solution and the transepithelial potential is clamped to the short-circuit state [1]. In their natural conditions, amphibia hardly ever live in Ringer-like solutions. This has major consequences for the transport of NaCl. At the low concentrations in the usual habitats of frogs and toads, uptake of both ions must be active. Under these conditions, the skin is very tight and displays a high electrical resistance. After mounting the skin in an Ussing chamber and incubating both sides with Cl^- Ringer solution, the electrical resistance may decrease drastically and a large passive Cl^- specific conductance (G^{Cl}) develops.

1. Transport at low environmental sodium chloride

Na^+ and Cl^- are reabsorbed by amphibian skin from solutions with less than 0.1 mM NaCl. In the case of Na^+, uptake occurs by the same mechanisms as at higher external concentrations [2], i.e. by means of influx into the epithelial cells via amiloride-sensitive Na^+ channels and subsequent active extrusion to the basolateral space by the Na^+–K^+-ATPase, which provides the essential part of energy driving the transport. Proton secretion by the skin, accomplished by an H^+-ATPase in apical membranes of the mitochondria-rich cells (MRC), participates in Na^+ uptake [3]. The resulting electrical coupling between the two transport functions affects Na^+ uptake under these conditions, but the contribution is certainly less than would qualify it as energizing the Na^+ transport [4]. Proton secretion leads to mucosal positive potentials of 40–50 mV in the absence of Na^+ uptake (after blocking the Na^+ channels with amiloride) [3] and hyperpolarizes the apical membrane by about this value. This is less than 20% of the driving force provided by the Na^+–K^+-ATPase, which can be estimated from the apical membrane potential difference of -90 mV and the intracellular Na^+

* Corresponding author.
E-mail address: W.Nagel@lrz.uni-muenchen.de (W. Nagel).

0005-2736/02/$ - see front matter
PII: S0005-2736(02)00593-X

concentration of 2–5 mM [5]. For maintaining electroneutrality, the coordinated uptake of Na^+ and secretion of protons may be essential, because uptake of Na^+ alone would depolarize the apical membrane and by that limit its own entry. It may be more appropriate, therefore, to consider the apparent coupling between Na^+ and proton fluxes as permissive rather than viewing the proton secretion as energizing.

Another transport system, independent of the Na^+–K^+-ATPase, is involved in the uptake of Cl^- from the usual freshwater habitats of frogs. For this ion, electroneutral exchange of Cl^- against bicarbonate originating from proton secretion in the apical membranes of MRC has been proposed [6]. Similar transport mechanisms have been proposed for other Cl^- absorptive epithelia (for review see Ref. [7]), but a final verification of the process is still missing. H^+-ATPase has been demonstrated exclusively in MRC in frog skin [8] and a number of other species (U. Katz, unpublished observations). However, its possible involvement in Cl^- transport must be established and cannot be inferred simply on the basis of the presence of the enzyme.

2. Transport at high (isotonic) sodium chloride

Amphibian skins incubated with NaCl-Ringer on both sides and short-circuited show variable transepithelial resistance. This property, first noted by Koefoed-Johnsen et al. [1] and attributed to the variability of Cl^- permeability, is related to long-term adaptation or location of the skin on the body surface [9]. Spontaneous variation among identically kept animals is large without evident reason. We have studied a great number of tissues from *R. temporaria*, *R. esculenta* and *R. pipiens*, in which G^{Cl} ranged from very small, <0.1 mS/cm^2, to 5–6 mS/cm^2. In skins of some amphibian species (*R. pipiens berlinieri*, *Xenopus laevis*), G^{Cl} is low and cannot be activated by any experimental means. The properties lacking under these conditions are unknown. Toad skins are comparable with frog skins in the variability of G^{Cl} under short-circuit conditions, but these tissues show a particular response on voltage perturbation [10], which is only occasionally observed in frog skins [11]. When toad skin is voltage-clamped to serosa-negative values of 30 mV or more, G^{Cl} dissipates completely. Voltage perturbation to serosa-positive voltages activates a conductive anion pathway with half time between 20 s and 2 min. This time course is too slow for voltage-sensitive channel gating, although the behavior could be modeled according to the Hodgkin–Huxley theory [12]. Computer modeling has excluded alteration of intracellular electrolyte composition [13]. The relationship of voltage-activated G^{Cl} and the clamping potential is sigmoidal with half-maximal and full activation at 40–60 and ~100 mV, respectively. Activation requires the presence of Cl^- in the mucosal solution and is not elicited by voltage clamping alone. Actually, the voltage perturbation itself has no activating effect [14]; the increase of G^{Cl} appears to result from the induced entry of Cl^-. This behavior resembles the activation patterns of ClC-O Cl^- channels [15,16], which are activated by the entry of Cl^- from the external side. These channels activate similarly slow as the voltage-activated Cl^- current in toad skin and might reflect the delayed opening in a larger population of channels. The presence of gated components in the voltage-activated Cl^- current is suggested by our observation of a Lorentzian component in the power density spectrum of current fluctuation [17,18], which is believed to reflect opening and closure of ion channels. The fluctuation occurs with corner frequency of about 50 Hz. Similar values were observed in whole-cell patch clamp analyses [19]. A detailed analysis of channel properties from transepithelial data has not been possible due to the lack of specific blockers. Rough estimates on the basis of simplifying assumptions suggest a single-channel conductance in the order of 1–5 pS [17].

The mechanisms that control G^{Cl} in the amphibian skin are not well understood. cAMP has been proposed as the main physiological regulator of the pathway [20]. Studies from our laboratory have shown that the influence of increased cellular cAMP is more complex, as application of membrane-permeable analogues of this messenger or its induction by forskolin eliminate the development of voltage-activated G^{Cl} [18,21,22]. Instead, voltage-insensitive opening of the pathway with increasing concentrations of cAMP is induced. We have proposed that the anion conductance pathway combines a slow, voltage-activated gating mechanism and the actual anion translocation pathway [23]. In this scheme, cAMP at high concentrations fixes the "gate" in an open state. The role of cAMP at low concentrations and after â-adrenergic agonists is less clear and might be species-dependent [20,24]. More distinct influence originates from signaling via α_1-adrenoceptors, which specifically inhibit the voltage-activated pathway without influence on the cAMP-induced open pathway [25]. The attempts to identify regulative elements in the pathway for Cl^- movement need more specific work, which has been impeded by the uncertainty of its morphological localization. The following discussion is mainly devoted to this issue.

3. Observations related to the pathway of chloride

The toad skin is a multilayered, heterocellular epithelium (Fig. 1). Subepithelial glands, which secrete Cl^- upon stimulation with â-adrenergic agonists [26], are easily eliminated from the cell layer after incubation with collagenase-containing solutions. Three structures remain as potential routes for passive Cl^- movement: principal cells (PC), MRC and tight junctions (TJ), which seal the paracellular space between these cells. PC cannot account for transepithelial Cl^- movement because the chloride conductance

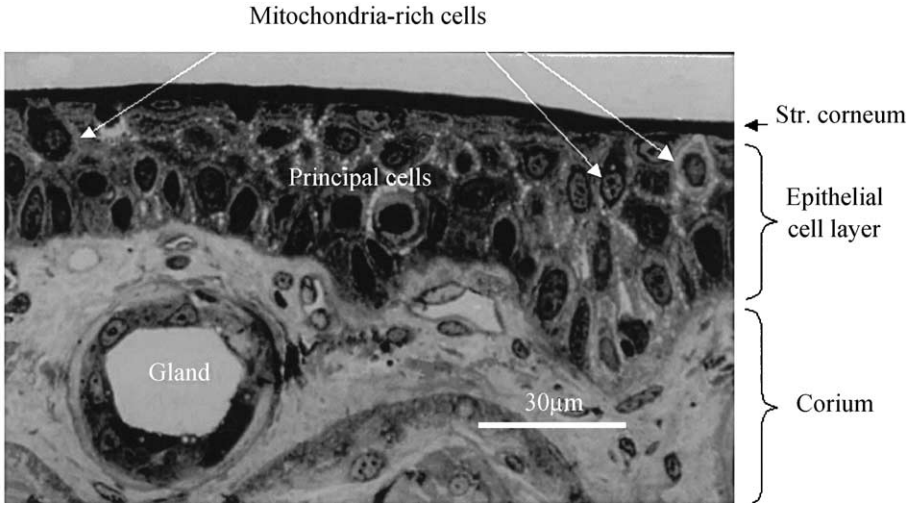

Fig. 1. Histology of the amphibian skin (from Ref. [46]).

of their membranes is negligible [23]. Thus, we deal with two putative locations of the pathway, which are both difficult to study in situ. TJ in the amphibian skin are covered by a dense layer of 2–3-μm thickness, the *stratum corneum*, and are neither accessible from the mucosal nor the serosal side. Furthermore, functional analysis of TJ permeability (as have been applied for cultured epithelia as MDCK, A6 and other cell lines) cannot be done in the amphibian skin. Most of our ideas rest on data from MRC, which are imbedded between the epithelial cells and covered by the stratum corneum. Difficulties due to this localization have hitherto prevented reproducible recording of intracellular potentials with microelectrodes and apparently also patch-clamp analysis in situ.

Patch-clamp studies have been done on individual MRC isolated by a combined enzymatic and mechanical procedure [19,27,28]. These studies demonstrate the presence of Cl^- selective channels in apical and basolateral membranes of the MRC. However, neither the characteristic time dependence of the chloride conductance after voltage perturbation nor the response to signaling factors was observed. Furthermore, the current carried by channels in the patched areas is orders of magnitude smaller than the Cl^- current of voltage-activated toad skin. This problem, which has been noted and discussed by the authors as well, might relate to damage during the isolation procedure. Trypsin, used for the separation of cells from the epithelial layer, inhibits the voltage-activated G^{Cl} [29]. Other reasons for failure will be discussed below.

4. In situ techniques for the analysis of MRC function

(1) A correlation between the density of MRC and Cl^- flux was reported by Voute and Meier [30] and has been used as an argument for the passage of Cl^- through these cells. Such correlations have subsequently been studied with different results ranging from perfect to near perfect linearity [31,32] to minimal or virtually absent dependency [9,11] between the density of MRC (D_{mrc}) and G^{Cl}. Such relationship implies that all MRC contribute equally to G^{Cl}, an unlikely condition, since MRC are not coordinated by intercellular coupling [33]. Observations with the vibrating probe [34] provide no evidence for the association of MRC and transepithelial anionic conductance. From the comparison of a number of species [9], it may be concluded that voltage-activated G^{Cl} is associated with MRC and cannot be elicited in their absence. But its dependence cannot be predicted and must be related to other, yet unknown factors.

(2) Swollen MRC have been observed after alteration of Cl^- transport in tissue sections by Voute and Meier [30] and are associated with Cl^- flux through these cells. Quantitative analyses have been made in frog and toad skin using video-enhanced micrometry [35–37]. Time-dependent changes of MRC volume after perturbation of Cl^- transport by different means including voltage-activation of G^{Cl} suggest a transcellular route for Cl^-. Considering the technical difficulties of analyzing the small changes of MRC volume after alteration of Cl^- transport, it must be questioned whether these data apply for all MRC or only to those particularly studied. The notion put forward by Foskett and Ussing [36] that the volume increased only in about 60% of frog skin MRC after voltage perturbation, demands a systematic reinvestigation of this problem.

(3) Electronprobe microanalysis of intracellular ion concentration was made to establish whether MRC take up bromide from the mucosal side when G^{Cl} is activated and a driving force for influx exists [11,38,39]. Bromide, which can be identified in the X-ray spectrum and is transported about as well as Cl^-, was indeed detected in some but not all MRC. The fraction of cells that exchanged a major part of bromide for Cl^- was 40–70%—even under conditions of high anion conductance, spontaneously existing or induced by stimulators or voltage perturbation, and large transepithelial bromide

movement. It was suggested that MRC exist in active or inactive state [39]. Morphologically, no difference between the two putative fractions has been reported.

(4) The voltage-activated G^{Cl} in the intact tissue has been localized by recording the Ohmic voltage drop of current flowing through activated sites in the solution above the source. The most capable technique for this analysis is the vibrating voltage probe used on toad skin by our groups [34,40] although other means to detect the voltage gradient in the solution have been applied [36]. All studies show an elevated current density in response to hyperpolarized voltage above or in the close vicinity of MRC, but only a fraction of MRC respond with current peaks. The ratio of active versus electrically silent MRC was between 15% [34] and some 30–80% [36,40], with several tissues showing no active sites at all [36,40]. A quantitative correlation between current flowing in peak regions and the clamping current demonstrated that less than 15% of the transepithelial current could be associated with active sites over MRC [34]. This observation has led to the conclusion that TJ between all epithelial cells should be responsible for the major fraction of voltage-activated Cl^- current, but the route could not be verified hitherto. Considering the uncertainty of assumptions underlying the quantification of local Cl^- current, we have applied more refined experiments and reanalyzed the previous conclusion.

5. The vibrating voltage probe

The distribution of local current densities was measured using a 2D vibrating probe (SVET, Applicable Electronics, Inc. Forestdale, MA, USA) as described previously [34]. A scheme of the technique is shown in Fig. 2. The high sensitivity of the system enables discrimination between two sites of elevated current density separated by about 25 μm [41]. In combination with appropriate optical resolution, this allows the identification of local current distribution in the toad skin. Isolated epithelia from skins of *Bufo viridis* were mounted in a miniature Ussing chamber with exposed area of 0.5 cm^2, which was assembled on the stage of an upright microscope. Both sides of the tissue were separately

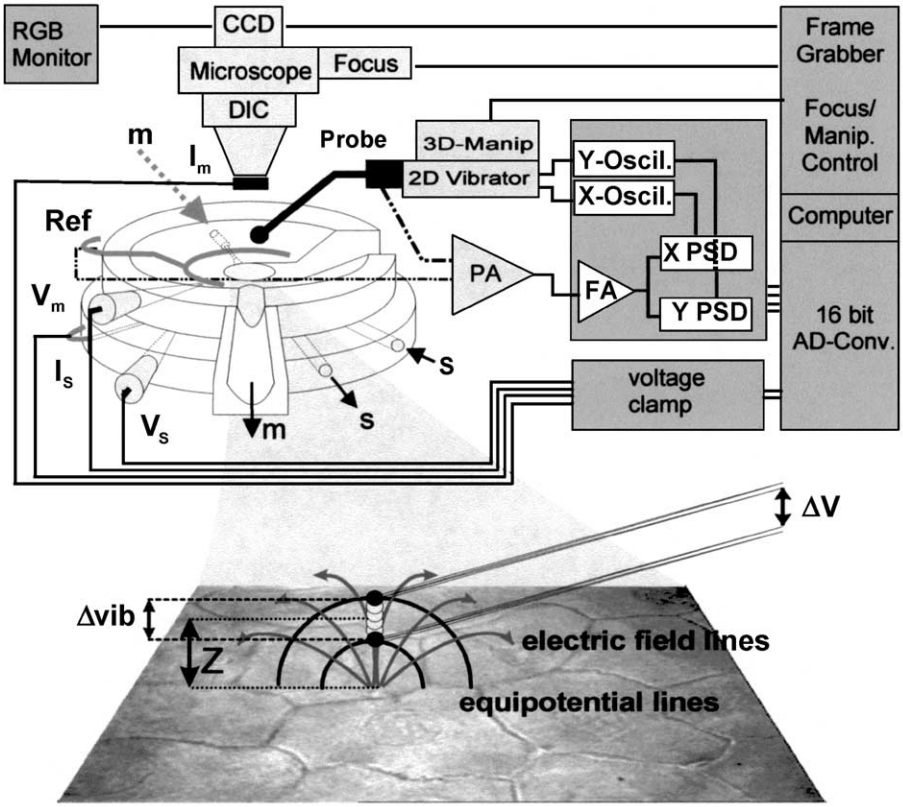

Fig. 2. Schematic drawing of the experimental set-up. The Ussing chamber is shown with the voltage and current sending electrodes (V_m, V_s, I_m, I_s) connected to the voltage clamp unit. Fluid inlets are labelled with arrows. The mucosal half chamber has an overflow directed by a cotton string. Perfusion of the serosal half chamber is gravity driven; slightly negative hydrostatic pressure at the serosal outlet fixes the tissue to a nylon grid without notable indentation. Local voltage gradients are recorded with a 2D-vibrating probe, mounted on a 3D micro-stepping motor manipulator. The vibrating probe system contains preamplifier (PA), filter amplifier (FA), phase-sensitive detectors (X-PSD, Y-PSD) and sine/cosine oscillators (*X*-Oscil., *Y*-Oscil.) controlled by the computer. The chamber is mounted on the stage of an upright microscope (Zeiss Axiovert 100 with 40 × /NA0.85 water-immersion lens) with Nomarski optics and a CCD camera connected to a RGB monitor and a frame grabber. The lower part shows the principle of vibrating electrode recording. Vibration of the electrode with amplitude Δvib at a mean distance of Z above the tissue measures a voltage drop ΔV at the probe tip generated by the ion flux. ΔV is converted into ion flux by adequate calibration.

perfused at 3–5 ml/min by gravity; the fluid of either half-chamber with volume of 0.2–0.3 ml could be exchanged within 30 s. The transepithelial potential difference (V_t) was recorded via KCl bridges close to the epithelial surfaces with Ag/AgCl electrodes. Chlorinated Ag plates maximally distant from the epithelium were used for voltage clamping. Particularly important for valid analyses is the homogeneity of the electrical field on the mucosal side. A custom-made silver grid, which covers the whole surface of the water immersion lens, served for this purpose. Voltage perturbation was made under computer control. The clamp current (I_t) was stored along with the data from the vibrating probe for quantitative correlation between I_t and local current density at the vibrating probe (I_p). The vibrating probe was calibrated in the Ussing chamber with a current source; this calibration was verified before and after the experiment by sending known magnitude of I_t through the chamber (without tissue) and recording I_p.

6. Distribution of voltage-activated chloride current in toad skin

When the optical focus is moved stepwise through the epithelial cell layer of a split skin, MRC are easily discerned as pear-shaped bodies with a small pole just below the cornified layer. Fig. 3A, taken at focus level 8 μm below the outer surface of the epithelium, shows the bodies of 29 MRC (marked with arrows), corresponding to a density of 140,000 MRC/cm^2. At a mean distance of about 30 μm between the individual MRC, the spatial resolution of the vibrating probe technique of about 25 μm would identify (shallow) peaks over the individual cells even if all MRC were active. The tissue was voltage-clamped to serosa +80 mV, which activated a current of 130 μA/cm^2. After stabilization of I_t, the surface was scanned in steps of 8 μm with the vibrating voltage probe. The current density profile (Fig. 3B) shows five to six sites of clearly elevated I_p; at some other positions, current density is slightly higher than the (blue) background level. This number of active sites is surprisingly small compared with the density of MRC. Current peaks are generally found at or in the immediate vicinity of MRC. The slight deviation between peaks and the actual site of MRCs may be due to imperfect identification of the apical pole of MRC. Most MRC are clearly *not* associated with elevated current density. This pattern is even more evident in the current density profile from the same area after the tissue was inactivated by clamping V_t to −30 mV followed by reactivation at +80 mV (Fig. 3C). This led to a slightly larger Cl^- current than before, but far fewer active sites are present in the chosen field. Large areas with background current are now detectable and contain many inactive MRC. These MRC, as well as their junctions with PC, show the same low current density as PC and their TJ.

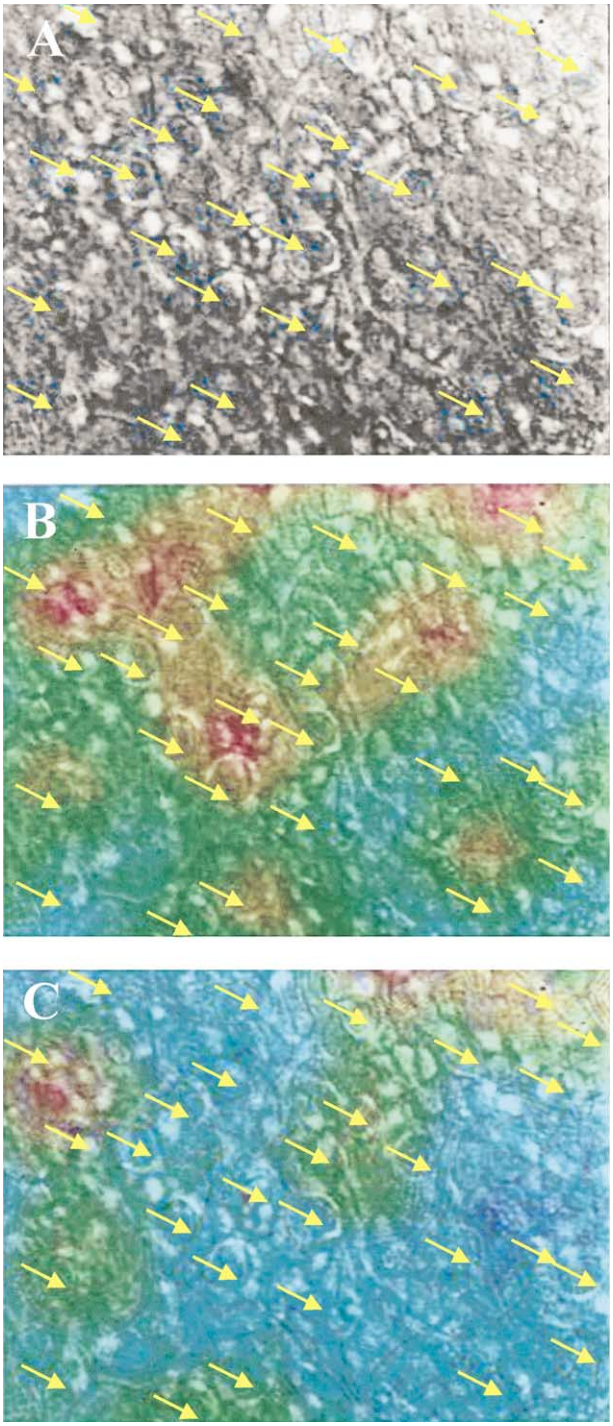

Fig. 3. Distribution of local current density in voltage-activated toad skin. (A) Video-image of the tissue (170 × 130 μm). MRC are marked by arrows. (B) Surface scan of current density distribution overlaid on the video-image of (A). Colour from blue to red corresponds to current density of 0 to 400 μA/cm^2. (C) Same as (B) after intermittent inactivation of G^{Cl}.

Whether TJ (between MRC/PC or among PC) are anion-permeable in areas of elevated current density cannot be discerned. Due to the stratum corneum, the vibrating probe cannot be advanced close enough to the apical poles of MRC for the required resolution [41].

We have scanned preparations from more than 20 toads repetitively for the local and temporal distribution of I_p. Invariably, individual sites of elevated current density were not fixed, but changed during periods of continuous voltage perturbation or upon de/reactivation of Cl^- current. Sites previously active became as tight as electrically inactive TJ between PC. Peaks were occasionally clustered over a group of few MRC, but that was the exception. The variability was easily perceived when few active peaks only emerged at alternating location from large areas of background level, but peaks appeared and disappeared also in tissues with elevated background. No morphological correlates of the activity of individual sites could be identified. In particular, we could never associate swollen MRC with elevated current density, nor has it been possible to identify the reason for the variability of the local voltage-activated Cl^- current. Theophylline or IBMX as well as membrane-permeable analogues of cAMP (CPT-cAMP), which increase G^{Cl} by two different mechanisms [22], do not change the behavior of active sites fundamentally. The elevated Cl^- current after stimulation with these agents is usually associated with a larger number of active sites, which renders the identification of individual peaks sometimes difficult. Nevertheless, the distribution is still not fixed and the number of peaks is always smaller than the density of MRC.

7. The effect of epinephrine on the current distribution

Epinephrine inhibits distinctively the voltage-activated G^{Cl} without affecting the cAMP-induced conductance. The effect is due to the interaction with α_1-adrenoceptors and involves liberation of Ca^{++} from intracellular stores [25]. Inhibition by epinephrine occurs at concentrations from less than 100 nM to more than 1 μM. This variability has prevented estimation of a half-maximal inhibitory concentration, and it was thus interesting to analyze whether epinephrine acts on I_p similarly variable. Fig. 4 shows the record of I_t and I_p over sites of high current density. At first, activation at an earlier identified active site was followed during conductance activation. The time course for the site current ($t_{1/2} = 16$ s) was

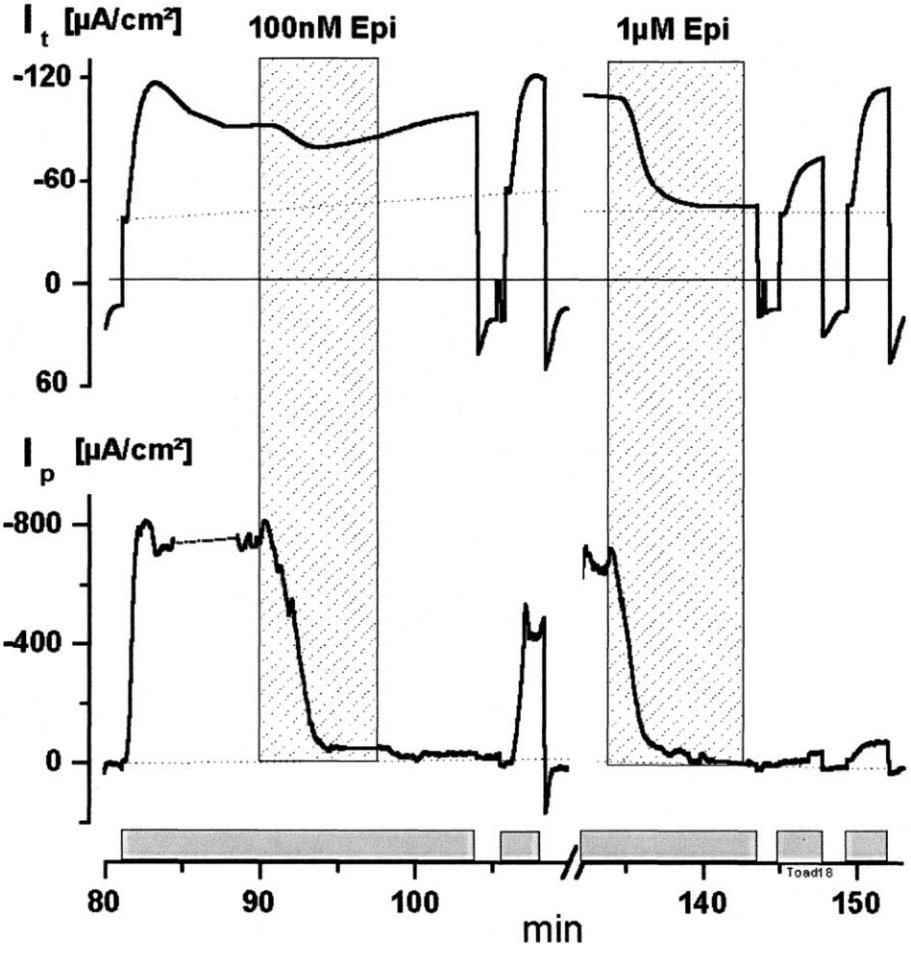

Fig. 4. Effect of epinephrine (Epi) on I_t and I_p. The shaded bars on the time scale indicate perturbation of V_t to +80 mV from a holding potential of −30 mV. The right part of the record was obtained from a different active site of the same tissue.

clearly faster than that of the clamp current ($t_{1/2}=31$ s). A current of 81 μA/cm^2 was activated in addition to the background current of 36 μA/cm^2. At the active site, a local current density of 800 μA/cm^2 was induced on top of the negligible current flowing before activation. Epinephrine (100 nM) reduced the voltage-activated I_t by about 15%; I_p decreased to the level of inactivation, i.e. was completely eliminated. Screening of the tissue (not shown) indicated that other sites were present with still elevated current density in the presence of epinephrine; this explains the low transepithelial efficiency. Washout of epinephrine returned I_p at the active site partially, whereas I_t was almost completely reversible. In the second part of Fig. 4, I_p was recorded at another site, because the first site terminated activity shortly after the period shown. At the concentration of 1 μm, epinephrine inhibited both voltage-activated I_t and I_p almost completely. Inhibition of local current was general, as no active site could be detected by scanning of the whole tissue area (not shown).

Similar observations have been made in a number of tissues. They demonstrate that most active sites are inhibited at 0.3–1 μM epinephrine. Lower concentrations caused variable inhibition, where it appears that active sites were either completely inhibited or not at all. Further studies will have to show whether this reflects "all-or-none" patterns. Areas of low I_p were not affected by epinephrine. This is illustrated in Fig. 5. In the control, two large and two to three minor peaks emerged from a clearly defined background level. The peaks disappeared after 1 μM epinephrine, but the background level was unchanged. Washout of epinephrine returned peaks at slightly different locations; the background level was invariant. This observation supports our view that areas of background level represent unspecific shunt current through inactive or inactivated MRC and TJ.

8. Effect of voltage on the time course and magnitude of activated current

The sigmoidal shape of the dependence between V_t and voltage-activated G^{Cl} [23] can be reproduced in I_p. Fig. 6 shows this behavior for one active site, which responded consistently on voltage perturbation. Activated local current at the site, over which the vibrating probe was centered at a distance of 2 μm from the surface, increased to almost 900 μA/cm^2 at 100 mV. At each perturbation voltage, I_p remained briefly at the level of inactivation. The time course of the subsequent activation was strongly voltage dependent; $t_{1/2}$ decreased from >45 s at 40 mV to ~ 10 s at 100 mV. These patterns, which are also detectable in I_t, agree with previous transepithelial observations (reviewed by Larsen [7]). The maximal current density at the respective V_t was used to calculate the voltage dependence of the apparent site conductance. This local voltage/conductance relationship, shown in the inset of Fig. 6, displays the sigmoidal function typically obtained in transepithelial studies for the voltage-activated G^{Cl}. Half-maximal activation occurred at 57 mV and the maximal level of 9.9 mS/cm^2 was approached at V_t between 80 and 90 mV (see below for calculation of site conductance). Similar values were obtained in three other experiments. This indicates that conductive sites are fully activated at these voltage levels.

9. The magnitude of local current peaks

The total current flowing at a single peak can be calculated when the distance between current source and probe is known. For chloride cells in the operculum, this formalism could be applied [42] and has also been used for a rough estimation of peak current in frog skin [36]. However, proper estimation of the distance between the

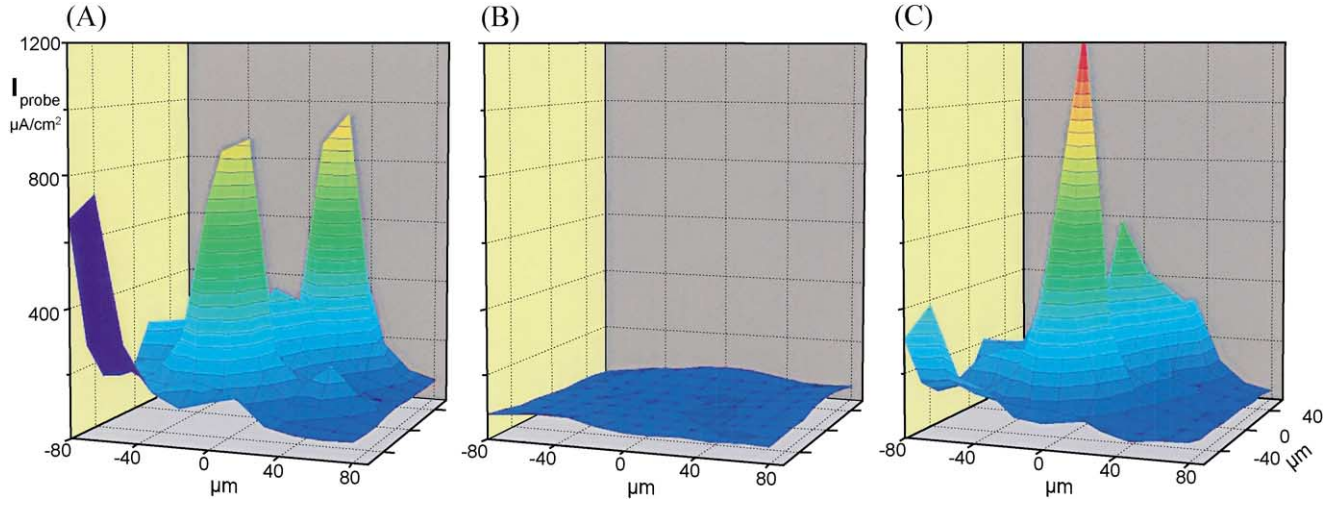

Fig. 5. 3D-contour plots of current density distribution under control conditions (A), during serosal application of 1 μM epinephrine (B) and after washout of epinephrine (C).

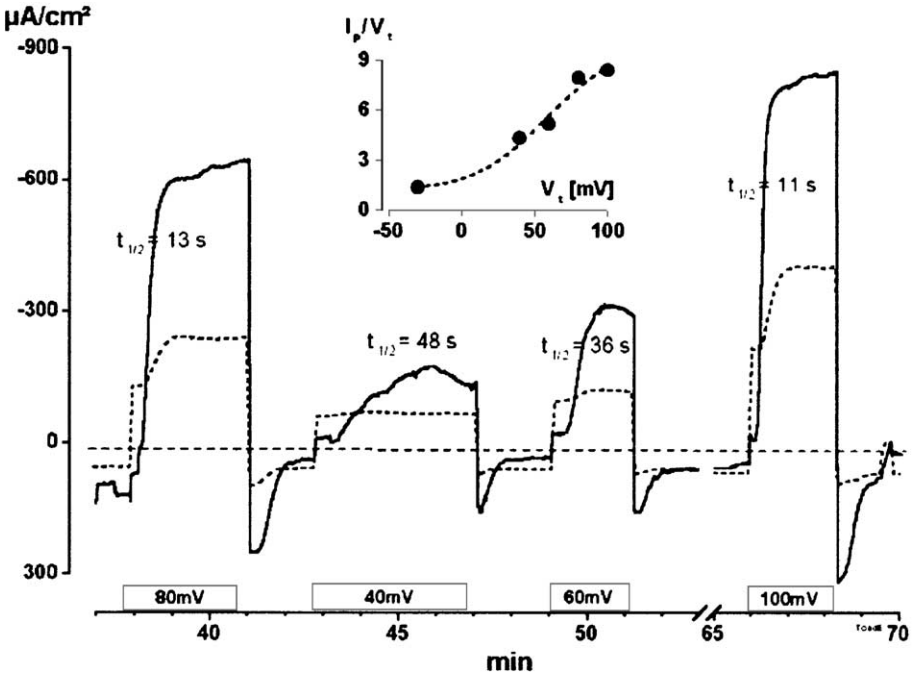

Fig. 6. Response of the I_p on the clamping potential. V_t was -30 mV between periods indicated by bars on the time scale. The dashed line shows the simultaneous recorded I_t. Steady state values of I_p, scaled by the respective clamping potential, are plotted versus V_t in the inset.

source and the center of the vibrating probe is not possible in amphibian skin due to the presence of the stratum corneum. Therefore, another approach was used to determine the total source current. It involves scanning a tissue area and inspecting peaks in the 3D-contour plot for rotational symmetry. For these identified peaks, current density on a line through the center of the source is extracted and fitted to a Gauss curve. The total site current is then obtained as the volume under the rotating bell. Fig. 7A shows an example of the procedure. In the depicted field, four sites of elevated current were identified by an area scan. From the scan data of the highest peak in the lower left corner, a peak current of 9.3 nA was calculated. As a further verification, the probe was positioned as close as possible above the surface in the center of the peak and then moved in steps of 4 μm to either side along a line (Fig. 7B). The observed current density profile is fairly well described by a Gauss bell curve with maximal current density of 1100 μA/cm^2 at the peak center. The half width of the peak is 25 μm. From these data a total peak current of 7.7 nA is obtained at the site, which is associated with one MRC (marked by the white arrow). The high degree of symmetry of the Gauss curve and the sharp decrease of current density above a second MRC close by (marked with a red arrow) indicates that this latter MRC does not contribute to the local current peak. Gauss curves can be derived for every peak detectable in an area scan or probed by a line scan. For reliable estimates, however, the correct magnitude of the baseline current must be known; erroneously elevated baseline level would reduce the total peak current. Due to the spread of current, few areas only in a field provide reliable baseline level. Selection of these usable sites is a matter of experience.

The results of our experiments are summarized as follows. At a clamp potential of 80 mV, we determined with line scans a current of 7.6 ± 2.2 nA ($n = 11$) at actives sites. The half-width of these sites was 24.5 ± 3.6 μm. Similar values are obtained from grid scans (peak current $= 8.0 \pm 3.6$ nA; half width $= 29 \pm 4.4$ μm; $n = 33$). The half-width of the peaks is about as expected for current originating from a single site < 15 μm in diameter [41]. Considering the dimensions of MRC and their average distance of about 30 μm, we can be sure that the current originates from single MRCs or their immediate surrounding. Application of Ohm's law to these data yields a conductance of about 100 nS at active sites. If the current flows through MRC with two membranes in series, conductance of each membrane has to be notably larger. This rather large value raises the question about the type of anion specific channels in both membranes of the MRC. Patch clamp analyses have shown the existence of Cl^- channels [27,28,43], but the density is orders of magnitude smaller than these estimates. It is possible that the technique to isolate the MRC reduced the viability or that spontaneously inactive MRC were selected. Recording of Cl^- channels from apical membranes of MRC could also be impossible due to the putative density of channels on the membrane. If the conductance of more than 100 nS derives from a single MRC, the apical membrane with an area of ≤ 10 μm^2 contains some 10^3–10^4 open Cl^- channels/μm^2 (assuming single channel conductance of 10–200 pS). Patches with such high con-

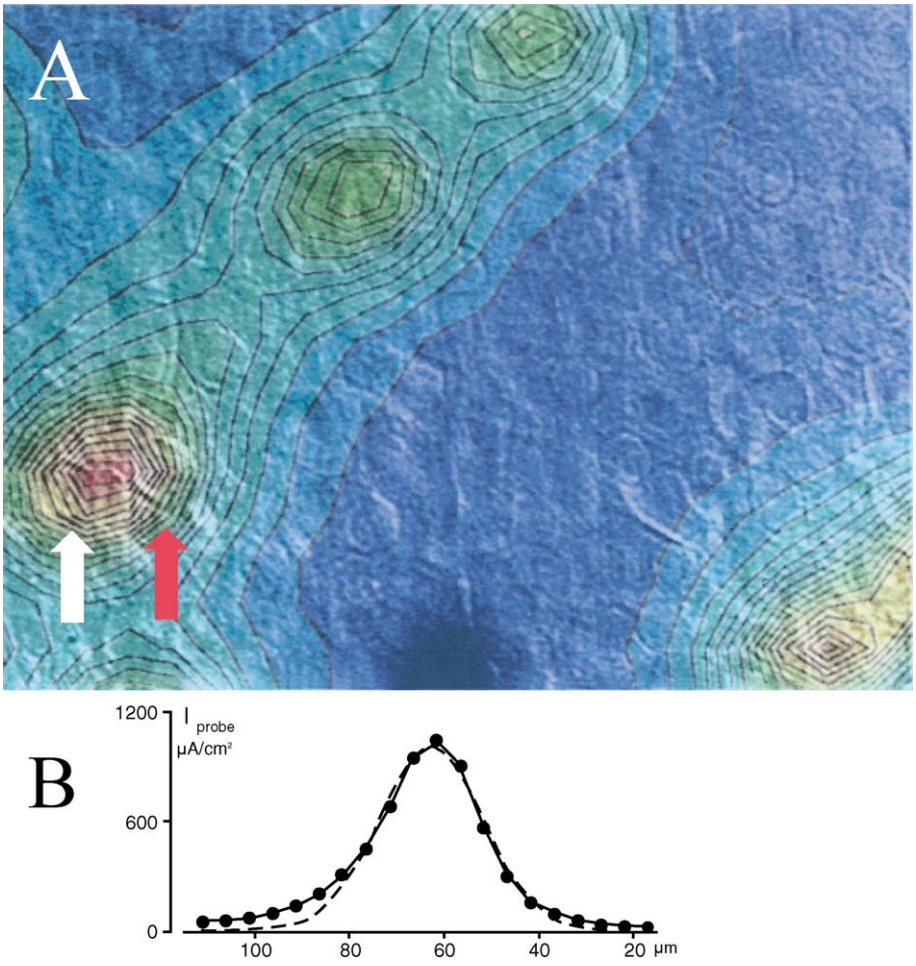

Fig. 7. (A) Distribution of local current density above an area of 170 × 130 μm^2, which was scanned in steps of 8 μm in *x*- and *y*-direction. Color-coding is from 0 (blue) to 1200 μA/cm^2 (red). Arrows point to two MRC at the location of high current density. (B) Current density profile of the active site. The dashed line represents the least square fit to a Gauss bell curve.

ductance and channel density are excluded as non-sealing or too noisy [44]. It may thus be surmised that reported patch clamp data relate to inactive apical membranes and may not definitely provide information on Cl^- channels of the voltage-activated pathway.

10. Current in active sites and transepithelial current

For comparison of local current with the I_t, the analysis of individual peaks is too subjective, because these peaks, often selected for the ease of evaluation, are most likely not representative for the area, which is already less than 1/1000 of the chamber area. Furthermore, the collection and calculation of the many peaks would be excessively time consuming. We have thus assumed that baseline current of identical magnitude flows all over the tissue area and any elevation is due to the existence of local current sites. Whether these sites are the MRC cannot be verified, but it appears likely in view of the localization. Our data cannot distinguish between current flowing through or around MRCs, because the spatial resolution is not sufficient [41]. TJ between MRC and PC could thus account for this particular Cl^- selective shunt pathway. The data on voltage-clamped individual MRC (Ref. [45] and preceding paper of this issue) suggest, on the other hand, a transcellular route through MRC for a significant fraction of the transepithelial Cl^- current. Existence of a similar pathway through the TJ appears unlikely. The problem is to find a proper estimate of the baseline current in inactive areas. This is easy if large continuous areas of low current density without peaks exist. Such areas are particularly evident in 3D-contour plots as shown in Fig. 5A–C. It is possible to test different aspects by rotation and to find out whether a low level reflects a base plateau. This baseline current, for which we have always seen voltage insensitivity, is subtracted from the sum of local currents in a field to yield the peak current. If the base plateau cannot be estimated due to spread of current from peaks, calculation is not possible. The major arguments prompting this procedure for baseline evaluation are (i) variable peak location, where the baseline declines after dissipation of a peak to the same low level as

Table 1
Quantitative analysis of current density in active sites relative to transepithelial voltage activated Cl^- current

D_{MRC} ($\times 10^3/cm^2$)	D_{peaks} ($\times 10^3/cm^2$)	$I_{single\ peak}$ (nA) (N/field)	I_{peaks} ($\mu A/cm^2$)	$I_{activated}$ ($\mu A/cm^2$)	$I_{peaks/act}$ (%)
101	32	5.4 (7)	177	245	72
87	14	7.3 (3)	101	130	78
89	33	5.2 (6)	155	175	89
127	19	8.8 (4)	170	140	121
110	22	6.6 (5)	150	170	88
106	18	7 (4)	120	80	150
86	15	8.3 (3)	124	165	75
110	10	4.5 (2)	54	90	60
116	11	7 (2)	79	93	85
260	59	5.3 (8)	319	320	100
110	17	11 (3)	184	185	99
63	8	8.2 (6)	68	110	62
96	14	5.8 (6)	80	140	57
143	4	6 (2)	26	50	52
87	31	2 (6)	59	125	47
112.8 ± 49.1	20.4 ± 14	6.6 ± 1.8	124.4 ± 70.7	147.9 ± 69.7	82.4 ± 25.6

Isolated skin from *B. viridis* was voltage-activated to serosa +80 mV.

in previously inactive zones, and (ii) the complete elimination of peak activity by epinephrine with unchanged baseline current density.

The results from 15 preparations that allowed clear identification of baseline current density are summarized in Table 1. The density of sites with elevated current density was $18 \pm 8\%$ of the MRC density; this fraction of "active" MRC is close to our previous estimate [34] and indicates that the majority of MRC is not in a conductive state. The average magnitude of current through active sites was 6.6 nA, but this value does not consider the coexistence of peaks of different size in scanned tissue areas. A rough estimate based on the maximal current density at the peak locations shows up to 15-nA current at individual sites. The background current density outside of peaks was slightly lower than the inactivated I_t of 65 ± 47 $\mu A/cm^2$ (observed immediately after perturbation to +80 mV). Current density in peak areas accounted for $82 \pm 26\%$ of the voltage-activated I_t. The scatter is large, but it must be considered that the calculation is based on less than 1/1000 of the tissue area in the chamber. Moreover, local and temporal variation of current density has large influence. We have frequently scanned areas lacking noteworthy elevated I_p; these observations were similarly excluded as those, which did not permit the guess of baseline current density. Although we cannot account for the entire transepithelial voltage-activated Cl^- current in the peak regions, detection of more than 80% on the average does not justify search for sites except those associated with MRC. The major challenge is now to verify the transcellular mode of passage and to identify the basis for the variability. This must be done in the intact epithelium, where the activity of the individual MRC can be confirmed, or should at least include procedure to ensure functional integrity of the cells.

Now that the voltage-activated G^{Cl} has been localized to MRC sites, the future investigation should deal with the molecular mechanism and proteins underlying this transport pathway. Studies must resolve the short-term control mechanisms responsible for activation/deactivation of individual sites (MRC) and its physiological significance. The fundamental differences between species need to be explained. This must be related to intricate control mechanisms together with other function(s) carried by MRCs in amphibian skin epithelium, as well as other tight epithelia.

Acknowledgements

We thank Mrs. Inge Kirmeyer for engaged assistance during the experiments and Dr. John Davis for critical reading of the manuscript. The work was financially supported by grants from the Deutsche Forschungsgemeinschaft.

References

[1] V. Koefoed-Johnsen, H. Levi, H.H. Ussing, The mode of passage of chloride ions through the isolated frog skin, Acta Physiol. Scand. 25 (1952) 150–163.
[2] J. Ehrenfeld, F. Garcia-Romeu, Kinetics of ionic transport across frog skin: two concentration-dependent processes, J. Membr. Biol. 56 (1980) 139–147.
[3] J. Ehrenfeld, F. Garcia-Romeu, Active hydrogen excretion and sodium absorption through isolated frog skin, Am. J. Physiol. 233 (1977) F46–F54.
[4] B.J. Harvey, Energization of sodium absorption by the H+-ATPase pump in mitochondria-rich cells of frog skin, J. Exp. Biol. 172 (1992) 289–309.
[5] W. Nagel, A. Dörge, The role of mitochondria-rich cells in sodium transport across amphibian skin, Pflügers Arch. 433 (1996) 146–152.
[6] E.H. Larsen, N.J. Willumsen, B.C. Christoffersen, Role of proton pump of mitochondria-rich cells for active transport of chloride ions in toad skin epithelium, J. Physiol. 450 (1992) 203–216.
[7] E.H. Larsen, Chloride transport by high-resistance heterocellular epithelia, Physiol. Rev. 71 (1991) 235–283.

[8] U. Klein, M. Timme, W. Zeiske, J. Ehrenfeld, The H+ pump in frog skin (*Rana esculenta*): identification and localization of a V-ATPase, J. Membr. Biol. 157 (1997) 117–126.
[9] U. Katz, A. Rozman, G. Zaccone, S. Fasulo, S. Gabbay, Mitochondria-rich cells in anuran Amphibia: chloride conductance and regional distribution over the body surface, Comp. Biochem. Physiol., A 125 (2000) 135–139.
[10] E.H. Larsen, P. Kristensen, Properties of a conductive cellular chloride pathway in the skin of the toad (*Bufo bufo*), Acta Physiol. Scand. 102 (1978) 1–21.
[11] W. Nagel, A. Dörge, Analysis of anion conductance in frog skin, Pflügers Arch. 416 (1990) 53–61.
[12] E.H. Larsen, B.E. Rasmussen, Membrane potential plays a dual role for chloride transport across toad skin, Biochim. Biophys. Acta 728 (1983) 455–459.
[13] E.H. Larsen, B.E. Rasmussen, Chloride channels in toad skin, Philos. Trans. R. Soc. Lond., B 299 (1982) 413–434.
[14] F. Lacaz-Vieira, J. Procopio, Comparative roles of voltage and Cl ions upon activation of a Cl conductive pathway in toad skin, Pflügers Arch. 412 (1988) 634–640.
[15] T.-Y. Chen, C. Miller, Nonequilibrium gating and voltage dependence of the CIC-O Cl^- channel, J. Gen. Physiol. 108 (1996) 237–250.
[16] M. Pusch, U. Ludewig, A. Rehfeldt, T.J. Jentsch, Gating of the voltage-dependent chloride channel CIC-O by the permeant anion, Nature 373 (1995) 527–530.
[17] W. Nagel, W. Van Driessche, Chloride-related fluctuation in frog skin, Pflügers Arch. 415 (1990) R30.
[18] W. Nagel, W. Van Driessche, Effect of forskolin on conductive anion pathways of toad skin, Am. J. Physiol. 263 (1992) C166–C171.
[19] E.H. Larsen, B.J. Harvey, Chloride currents of single mitochondria-rich cells of toad skin epithelium, J. Physiol. 478 (1994) 7–15.
[20] N.J. Willumsen, L. Vestergaard, E.H. Larsen, Cyclic AMP- and b-agonist-activated chloride conductance of a toad skin epithelium, J. Physiol. 449 (1992) 641–653.
[21] A. Rozman, S. Gabbay, U. Katz, Chloride conductance across toad skin: effects of ionic acclimation and cAMP and relation to mitochondria-rich cells, J. Exp. Biol. 203 (2000) 2039–2045.
[22] U. Katz, W. Nagel, Effects of cyclic AMP and theophylline on chloride conductance across toad skin, J. Physiol. (Lond.) 489 (1995) 105–114.
[23] W. Nagel, J.M. Davis, U. Katz, Transepithelial chloride conductance in amphibian skin: regulatory mechanisms and localization, Pflügers Arch. 440 (2000) 797–808.
[24] A. Rozman, U. Katz, Effect of cAMP on the voltage-activated chloride conductance across frog skin (*Rana pipiens*), Comp. Biochem. Physiol., A 132 (2002) S60.
[25] W. Nagel, U. Katz, α_1-Adrenoceptors antagonize activated chloride conductance of amphibian skin epithelium, Pflügers Arch. 436 (1998) 863–870.
[26] I.G. Thompson, J.W. Mills, Isoproterenol-induced current changes in glands of frog skin, Am. J. Physiol. 241 (1981) C250–C257.
[27] N.J. Willumsen, E.H. Larsen, Identification of anion-selective channels in the basolateral membrane of mitochondria-rich epithelial cells, J. Membr. Biol. 157 (1997) 255–269.
[28] J.B. Sørensen, E.H. Larsen, Heterogeneity of chloride channels in the apical membrane of isolated mitochondria-rich cells from toad skin, J. Gen. Physiol. 108 (1996) 421–433.
[29] W. Nagel, U. Katz, Trypsin inhibits voltage-activated chloride conductance of toad skin, Comp. Biochem. Physiol. 122 (1999) 109–115.
[30] C.L. Voute, W. Meier, The mitochondria-rich cell of frog skin as hormone-sensitive "shunt-path", J. Membr. Biol. 40 (1978) 151–165.
[31] N.J. Willumsen, E.H. Larsen, Cl currents in toad skin: potential dependence and relation to mitochondria-rich cell density, in: R. Gilles, M. Gilles-Baillien (Eds.), Transport Processes, Ion- and Osmoregulation, Springer Verlag, Berlin, 1985, pp. 20–30.
[32] O. Devuyst, V. Beaujean, J. Crabbe, Effects of environmental conditions on mitochondrial rich cell density and chloride transport in toad skin, Pflügers Arch. 417 (1991) 577–581.
[33] R. Rick, A. Dörge, E. von Arnim, K. Thurau, Electron microprobe analysis of frog skin epithelium: evidence for a syncytial sodium transport compartment, J. Membr. Biol. 39 (1978) 313–331.
[34] W. Nagel, P. Somieski, A.M. Shipley, Mitochondria-rich cells and voltage-activated chloride current in toad skin epithelium, J. Membr. Biol. 161 (1998) 131–140.
[35] K.R. Spring, H.H. Ussing, The volume of mitochondria-rich cells of frog skin epithelium, J. Membr. Biol. 92 (1986) 21–26.
[36] J.K. Foskett, H.H. Ussing, Localization of chloride conductance to mitochondria-rich cells in frog skin epithelium, J. Membr. Biol. 91 (1986) 251–258.
[37] E.H. Larsen, H.H. Ussing, K.R. Spring, Ion transport by mitochondria-rich cells in toad skin, J. Membr. Biol. 99 (1987) 25–40.
[38] A. Dörge, R. Rick, F.X. Beck, W. Nagel, Uptake of Br in mitochondria-rich and principal cells of toad skin epithelium, Pflügers Arch. 412 (1988) 305–313.
[39] R. Rick, Short-term bromide uptake in skins of *Rana pipiens*, J. Membr. Biol. 138 (1994) 171–179.
[40] U. Katz, C. Scheffey, The voltage-dependent chloride current conductance of toad skin is localized to mitochondria-rich cells, Biochim. Biophys. Acta 861 (1986) 480–482.
[41] P. Somieski, W. Nagel, Localizing transepithelial conductive pathways using a vibrating voltage probe, J. Exp. Biol. 201 (1998) 2489–2495.
[42] J.K. Foskett, T.E. Machen, Vibrating probe analysis of teleost opercular epithelium: correlation between active transport and leak pathways of individual chloride cells, J. Membr. Biol. 85 (1985) 25–35.
[43] N.J. Willumsen, E.H. Larsen, Chloride channels in the basolateral membrane of mitochondria-rich cells of toad skin epithelium, J. Physiol. 489.P (1995) 116–117.
[44] N.J. Willumsen, J. Amstrup, E.H. Larsen, Chloride ion translocation across mitochondria-rich cell membranes in amphibian skin, Comp. Biochem. Physiol., A 132 (2002) S51–S52.
[45] E.H. Larsen, S. Nedergaard, N.J. Willumsen, Role of mitochondria-rich cells for passive chloride transport, with a discussion of Ussing's contribution to our understanding of shunt pathways in epithelia, J. Membr. Biol. 184 (2001) 247–254.
[46] M.G. Farquhar, G.E. Palade, Cell junctions in amphibian skin, J. Cell Biol. 26 (1965) 263–291.